



# Surface CO<sub>2</sub> parameters and air–sea CO<sub>2</sub> flux distribution in the eastern equatorial Atlantic Ocean

Urbain Koffi<sup>a,b</sup>, Nathalie Lefèvre<sup>a,\*</sup>, Georges Kouadio<sup>b</sup>, Jacqueline Boutin<sup>a</sup>

<sup>a</sup> LOCEAN, UMR 7159 IRD/CNRS/UPMC/MNHN, Université Pierre et Marie Curie, Case 100, 4 place Jussieu, 75252 Paris cedex 05, France

<sup>b</sup> Laboratoire de Physique de l'Atmosphère et de Mécanique des fluides, Université d'Abidjan Cocody, 01 b.P.V 34 Abidjan 01 Côte d'Ivoire

## ARTICLE INFO

### Article history:

Received 25 September 2009

Received in revised form 9 April 2010

Accepted 13 April 2010

Available online 24 April 2010

### Keywords:

Eastern equatorial Atlantic

CO<sub>2</sub> flux

Alkalinity

Dissolved inorganic carbon

## ABSTRACT

Six cruises have been carried out in the eastern equatorial Atlantic between June 2005 and September 2007 to study the distribution of the surface total alkalinity (TA) and dissolved inorganic carbon (DIC). During these cruises a strong north–south gradient is observed in sea surface temperature (SST), sea surface salinity (SSS), DIC and TA. Low surface salinity waters are associated with low TA and low DIC. They are observed north of the equator (0°–6°N) in the Guinea current, whereas higher concentrations are observed south of the equator. TA–SSS and DIC–SST–SSS relationships are determined and are used to calculate surface fCO<sub>2</sub>. Monthly maps of fCO<sub>2</sub> are obtained, on a one degree grid, using SST and SSS fields for the region 10°W–10°E, 6°N–10°S from June to November. The monthly mean flux of CO<sub>2</sub> ranges from 1.69 ± 1.94 mmol m<sup>-2</sup> day<sup>-1</sup> in November to 2.78 ± 1.65 mmol m<sup>-2</sup> day<sup>-1</sup> in August over the region. Using the same gas exchange coefficient, the CO<sub>2</sub> flux was calculated with the climatological ΔfCO<sub>2</sub>. Our estimates show a stronger gradient between northern and southern waters than the climatology, probably due to a lack of data in the climatology as well as its 4° latitude by 5° longitude resolution.

© 2010 Elsevier B.V. All rights reserved.

## 1. Introduction

Estimating the sources and sinks of the atmospheric CO<sub>2</sub> is important for understanding the role of the ocean with respect to the atmospheric increase. Oceanic inversions, atmospheric inversions and estimates based on oceanic observations converge to a mean CO<sub>2</sub> outgassing of the order of 0.7 GtC year<sup>-1</sup> (1.8 mmol m<sup>-2</sup> day<sup>-1</sup>) for the tropical oceans (Denman et al., 2007), the tropical Pacific being the largest source of CO<sub>2</sub> for the atmosphere. The estimates of the CO<sub>2</sub> flux of the tropical Atlantic show a large range of variability. For the latitudinal band 14°N–14°S, using a global carbon model, Gruber et al. (2009) found a mean flux of 0.12 PgC yr<sup>-1</sup> (0.31 mmol m<sup>-2</sup> day<sup>-1</sup>) for the 1990s and the early 2000 with differences between the flux estimates across models reaching 0.08 PgC year<sup>-1</sup> (0.20 mmol m<sup>-2</sup> day<sup>-1</sup>). Similar results are obtained by Baker et al. (2006) over the 1991–2000 period. Based on interpolation of CO<sub>2</sub> observations, the monthly climatology built by Takahashi et al. (2009) shows that this region is a source of CO<sub>2</sub> to the atmosphere of 0.10 PgC year<sup>-1</sup> (0.26 mmol m<sup>-2</sup> day<sup>-1</sup>) on annual average.

In order to better constrain the CO<sub>2</sub> flux, it is important to monitor the CO<sub>2</sub> variability in the tropical Atlantic. Several cruises have been conducted in this region, providing estimates of the air–sea CO<sub>2</sub> flux. From 1982 to 1984, the Focal cruises sampled the eastern equatorial

Atlantic along the 4°W, 22°W and 35°W sections between 5°N and 5°S for January–February and July–August (Andrié et al., 1986). They estimated a mean CO<sub>2</sub> flux of 0.05 ± 0.10 mmol m<sup>-2</sup> day<sup>-1</sup> in January–February 1983 and 0.31 ± 0.53 mmol m<sup>-2</sup> day<sup>-1</sup> in July–August 1983 along 4°W. One year after, the mean fluxes were respectively 0.97 ± 1.21 mmol m<sup>-2</sup> day<sup>-1</sup> in January–February 1984 and 0.40 ± 0.73 mmol m<sup>-2</sup> day<sup>-1</sup> in July–August 1984 along the same section, which highlights the high temporal variability occurring in this area. Oudot et al. (1995) compared their estimates with data collected 10 years after, during the Cither 1 cruise. The mean flux was higher with a value of 1.62 ± 2.12 mmol m<sup>-2</sup> day<sup>-1</sup> in January–March 1993 along 4°W but the temporal variability is high so it is not clear whether the source of CO<sub>2</sub> is increasing with time. In June 2006, the CO<sub>2</sub> flux estimated in the eastern tropical Atlantic (10°S–6°N; 10°W–10°E) was 2.39 ± 2.41 mmol m<sup>-2</sup> day<sup>-1</sup> (Lefèvre, 2009). The large range of estimates of the air–sea CO<sub>2</sub> flux might be explained by the undersampling and the high natural variability in the eastern equatorial Atlantic.

In this paper, we describe the variability of dissolved inorganic carbon (DIC) and alkalinity (TA) measured during six cruises performed from 2005 to 2007 in the eastern equatorial Atlantic (10°S–10°N, 10°E–10°W). As sea surface temperature (SST) and sea surface salinity (SSS) are more frequently and regularly measured than DIC and TA, we examine whether these parameters could be used as proxies to describe the spatial and temporal variability of DIC and TA. Empirical relationships relating TA, DIC to these parameters are determined and monthly maps of the fugacity of CO<sub>2</sub> (fCO<sub>2</sub>) are

\* Corresponding author. Tel.: +33144273821; fax: +33144277159.

E-mail address: [nathalie.lefevre@ird.fr](mailto:nathalie.lefevre@ird.fr) (N. Lefèvre).

constructed from climatological SST and SSS fields. Air–sea  $\text{CO}_2$  fluxes are then calculated and compared to the ones derived from the  $\text{fCO}_2$  climatology of Takahashi et al. (2009).

## 2. Data and methods

From June 2005 to September 2007, six oceanographic cruises (Fig. 1), EGEE (for “étude de la circulation océanique et de sa variabilité dans le golfe de Guinée”), took place in the eastern equatorial Atlantic with two cruises per year (Table 1). These oceanographic cruises were part of the oceanic component of the

international AMMA (African Monsoon Multidisciplinary Analyses) program. The cruises have been conducted in June and in September starting from, and ending in, Cotonou (Benin). Each cruise consisted of two legs. The first leg extended over the first two weeks of the month and the second leg on the last two.

195 samples of surface seawater were collected for DIC and TA analyses. Temperature and salinity were also measured on the same seawater as the samples for DIC and TA. The samples were poisoned with a saturated  $\text{HgCl}_2$  solution. DIC and TA were measured using potentiometric titration derived from the method developed by Edmond (1970) with a closed cell. The calculations of the equivalent

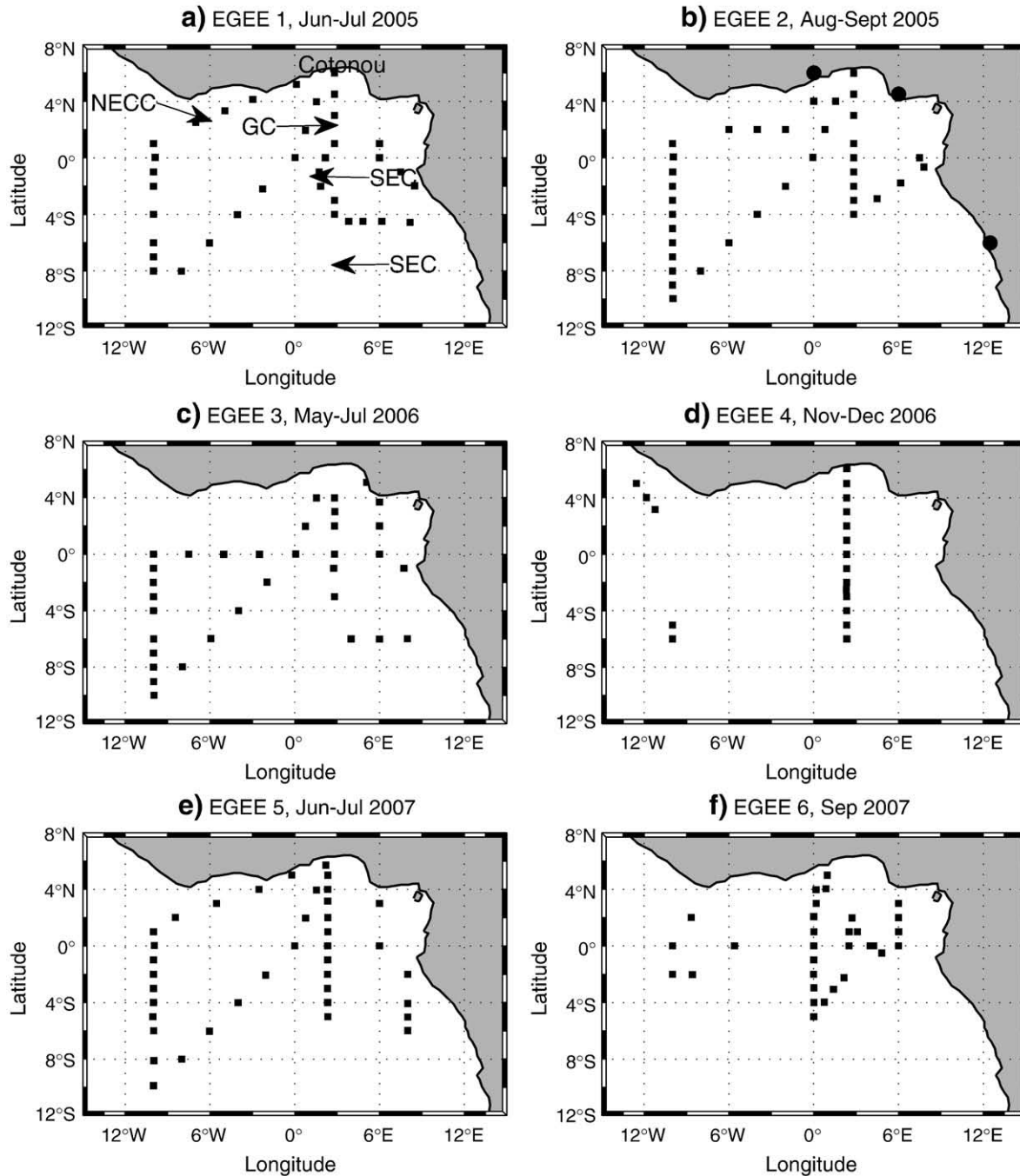


**Fig. 1.** Location of TA and DIC samples during a) EGEE 1 (7 June–6 July 2005), b) EGEE 2 (29 August–30 September 2005), c) EGEE 3 (27 May–7 July 2006), d) EGEE 4 (19 November–1 December 2006), e) EGEE 5 (6 June–3 July 2007) and f) EGEE 6 (1–30 September 2007) cruises. The main surface currents are indicated on panel a) and correspond to the North Equatorial Counter Current (NECC), The Guinea Current (GC), and the South Equatorial Current (SEC). The Congo (6°S, 12°E), Niger (3°N, 8°E) and Volta (4°N, 0°) river mouths are indicated with filled circles on panel b).

**Table 1**

Dates of EGEE cruises in the eastern equatorial Atlantic from June 2005 to September 2007.

Cruises	Dates
EGEE 1	7 June–6 July 2005
EGEE 2	29 August–30 September 2005
EGEE 3	27 May–7 July 2006
EGEE 4	19 November–1 December 2006
EGEE 5	6 June–3 July 2007
EGEE 6	1–30 September 2007

points were estimated using a non-linear regression method (DOE, 1994). For calibration, we used the Certified Reference Materials (CRMs) provided by Prof. A. Dickson (Scripps Institution of Oceanography, San Diego, USA). The accuracy of DIC and TA were estimated at  $\pm 2 \mu\text{mol kg}^{-1}$ . During EGEE 3  $f\text{CO}_2$  was measured underway (Lefèvre, 2009) but during the other cruises pH and  $f\text{CO}_2$  were not measured so that the carbon system can only be determined using DIC and TA. The underway  $f\text{CO}_2$  measurements were used to determine the best set of dissociation constants for the calculation of  $f\text{CO}_2$  at stations where DIC and TA were measured, and to validate  $f\text{CO}_2$  derived from our extrapolated DIC and TA all along the track of the EGEE 3 cruise.

Additional DIC observations from the ANTXI/1&5 cruises and TA observations from ARAMIS cruise were used. ANTXI/1&5 cruises were carried out respectively in October–November 1993 and in May–June 1994 on board the R.V. Polarstern between  $48^\circ\text{N}$  and  $29^\circ\text{S}$  (Bakker et al., 1999). The ARAMIS cruises occurred in October 2005, May 2006 and April 2007 from France to Brazil on board the Monte Olivia. They cross the equator around  $25^\circ\text{W}$  between  $20^\circ\text{N}$  and  $20^\circ\text{S}$  (Tanguy et al., 2010).

The air–sea  $\text{CO}_2$  flux has been calculated with the following expression:  $F = K \cdot \Delta f\text{CO}_2$  where  $K$  is the gas exchange coefficient and  $\Delta f\text{CO}_2$  the difference between seawater  $f\text{CO}_2$  and atmospheric  $f\text{CO}_2$ . Atmospheric  $f\text{CO}_2$  is calculated from the monthly  $\text{CO}_2$  molar fraction recorded at the Ascension Island at  $7.92^\circ\text{S}$ ,  $14.42^\circ\text{W}$  from 2005 to 2007. The mean value is  $373.2 \pm 0.75 \mu\text{atm}$ .  $K$  is the weekly mean  $\text{CO}_2$  exchange coefficient derived from QuikSCAT wind speeds using the quadratic relationship of Sweeney et al. (2007) at a spatial resolution of  $1^\circ \times 1^\circ$  (Boutin et al., 2009). The monthly flux and the annual flux derived from the EGEE relationships have been calculated at a spatial resolution of  $1^\circ \times 1^\circ$ .

### 3. Hydrological situation

The surface layer of the tropical Atlantic is occupied by warm Tropical Surface Water (TSW) and underneath lies the South Atlantic Central Water (Stramma and Schott, 1999). The main surface current is the South Equatorial current (SEC) that flows westward and extends from the surface to about 100 m. It is found between approximately  $4^\circ\text{N}$  and  $15\text{--}25^\circ\text{S}$  depending on the longitudinal location and on the time of the year. Equatorial upwelling and coastal upwelling along the eastern boundary merge to form a cold tongue during the main upwelling season, and the cold tongue is advected westward by the SEC. This cold tongue transports  $\text{CO}_2$  rich waters and  $f\text{CO}_2$  increases as surface water warms up toward the west (Andrié et al., 1986). Further north ( $>2^\circ\text{N}$ ), there is the Guinea Current (GC), an eastward, shallow, surface flow, fed by the North Equatorial counter current (NECC) off the Liberian coast. Its average depth is 15 m near the coast and 25 m offshore. Although the location of the NECC changes seasonally according to the position of ITCZ, the position of the GC remains fairly constant (Binet and Marchal, 1993) and the northern tropical convergence along about  $3^\circ\text{N}$  separates the GC from the SEC. The Guinea current carries low salinity waters as a result of the high precipitation and numerous rivers in the eastern

Gulf of Guinea (Hardman-Mountford and McGlade, 2003). A seasonal coastal upwelling occurs between Cape Palmas ( $8^\circ\text{W}$ ) and Cotonou ( $2^\circ\text{E}$ ) in the northern part of the Gulf of Guinea, but the area affected by this upwelling is a narrow band close to the coast. We do not consider this coastal upwelling here because very few samples were collected in this region.

During the EGEE cruises, the salinity varies between 32 and 37 and the temperature between  $21^\circ\text{C}$  and  $30^\circ\text{C}$  over the region  $10^\circ\text{S}\text{--}6^\circ\text{N}$ ,  $10^\circ\text{W}\text{--}10^\circ\text{E}$ . A north ( $6^\circ\text{N}\text{--}0^\circ$ )–south ( $0^\circ\text{--}10^\circ\text{S}$ ) gradient appears both in salinity and temperature, with relatively low salinity and relatively high temperature north of the equator, and relatively high salinity and low temperature south of the equator. In the warm water transported by the GC north of the equator, SSS is relatively low ( $34.91 \pm 0.66$ ) because this region is subject to river discharge. In particular, the Niger and Volta rivers (Fig. 1b) supply freshwater. From the equator to  $10^\circ\text{S}$ , away from the coast, saltier (averaged SSS  $35.71 \pm 0.41$ ) and colder waters ( $\text{SST} < 26^\circ\text{C}$ ) are observed, which is due to the influence of the upwelling occurring from July to September. This feature, observed during each EGEE cruise, is illustrated for the EGEE 5 cruise along  $2^\circ\text{E}$  (Fig. 2) because this section was the most sampled. Another area of low salinity (33.90) is observed near the Congo River mouth at  $6^\circ\text{S}$ ,  $8^\circ\text{E}$  in June 2007.

### 4. Distribution of carbon parameters

#### 4.1. TA distribution

The surface TA measurements have a large range of variability (as large as  $290 \mu\text{mol kg}^{-1}$ ) with values varying from  $2115 \mu\text{mol kg}^{-1}$  at  $3^\circ\text{N}$ ,  $6^\circ\text{E}$  (Sep. 2007) to  $2405 \mu\text{mol kg}^{-1}$  at  $10^\circ\text{S}$ ,  $10^\circ\text{W}$  (June 2007). The highest alkalinity values ( $>2300 \mu\text{mol kg}^{-1}$ ) are associated with relatively low temperatures ( $<26^\circ\text{C}$ ) and high salinity ( $>35$ ), and are observed mainly in the SEC. The lowest alkalinity values ( $<2300 \mu\text{mol kg}^{-1}$ ) are associated with high temperature ( $26\text{--}30^\circ\text{C}$ ) and low salinity (32–35) in the GC.

Along  $2^\circ\text{E}$ , the distribution of TA is similar to salinity with a north–south gradient (Fig. 3a). Averaged TA values vary from  $2282 \pm 26 \mu\text{mol kg}^{-1}$  north of the equator to  $2337 \pm 37 \mu\text{mol kg}^{-1}$  south of the equator. To remove the salinity effect, TA values are normalized to a salinity of 35 ( $\text{NTA} = \text{TA} \cdot 35 / \text{SSS}$ ). The north–south TA gradient disappears after this normalization, which means that TA is fully explained by the SSS variations resulting from dilution.

When averaged over all longitudes, north of the equator, the mean TA value ranges from  $2285 \pm 33 \mu\text{mol kg}^{-1}$  in September to  $2292 \pm$

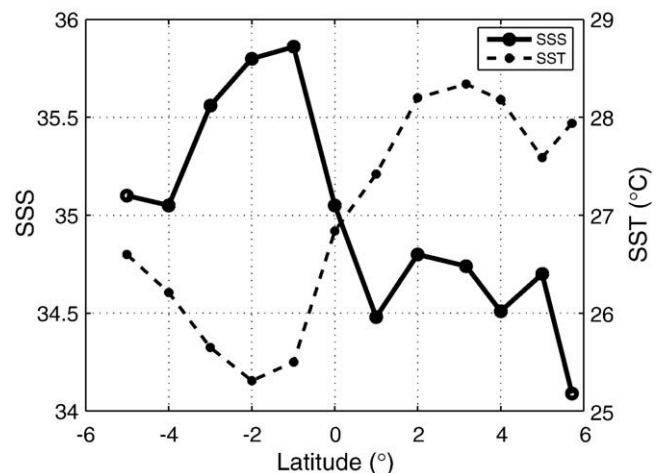


**Fig. 2.** Distribution of sea surface salinity and sea surface temperature between  $6^\circ\text{S}$  and  $6^\circ\text{N}$  along  $2^\circ\text{E}$  during EGEE 5 in June 2007.

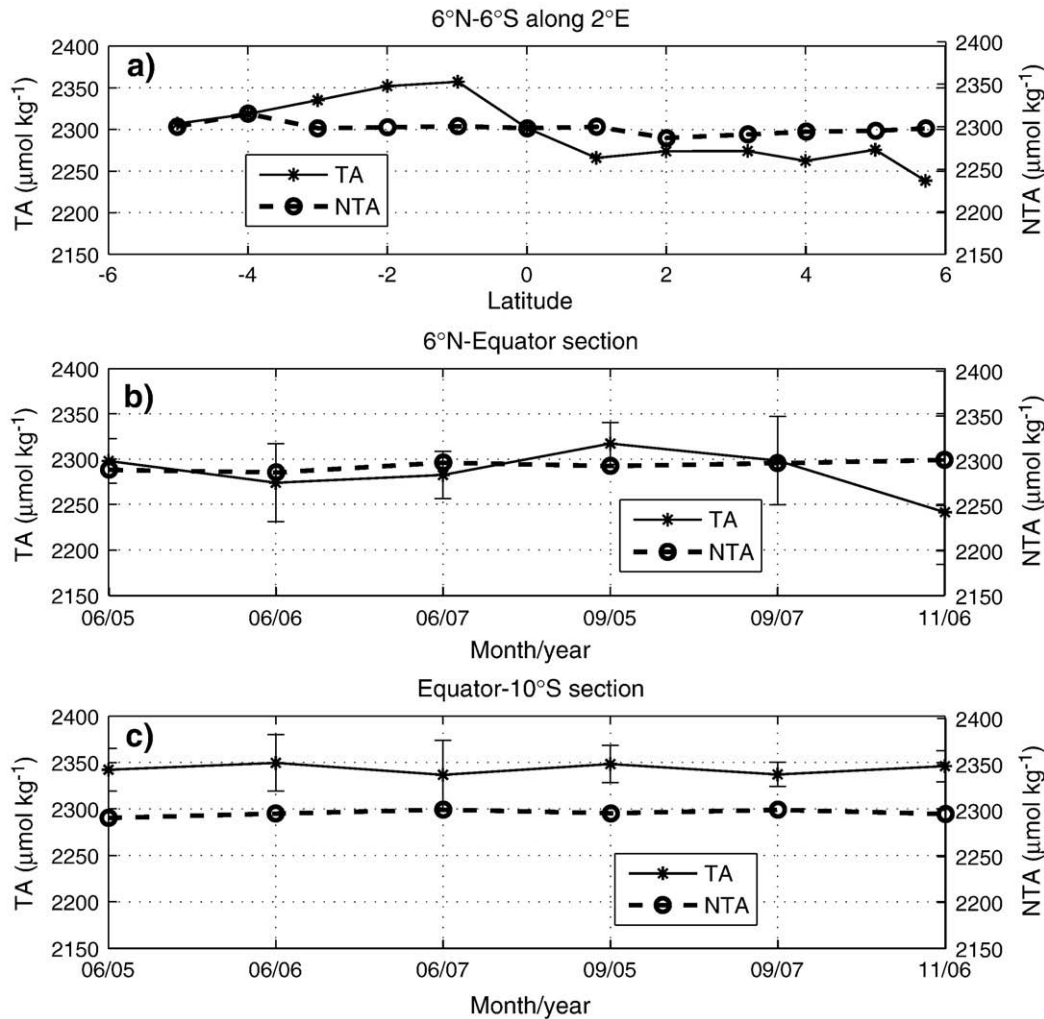


**Fig. 3.** a) Distribution of alkalinity (TA) and normalized alkalinity (NTA) between 6°N and 6°S during EGEE 5 in June 2007 along 2°E. b) Time variability of TA and NTA from 6°N to the equator and c) from the equator to 10°S. Standard deviation ( $\pm 1\sigma$ ) is indicated by vertical bars.

52  $\mu\text{mol kg}^{-1}$  in June (Fig. 3b). South of the equator, the mean TA value ranges from  $2342 \pm 31 \mu\text{mol kg}^{-1}$  in September to  $2345 \pm 18 \mu\text{mol kg}^{-1}$  in June (Fig. 3c). North and south of the equator, the mean TA values are similar in June and in September. Along 2°E, NTA values are almost constant showing that TA variations are fully explained by SSS variations.

#### 4.2. DIC distribution

During the EGEE cruises, DIC concentrations increase from about 1834 to 2085  $\mu\text{mol kg}^{-1}$  between 6°N and 10°S. The highest DIC concentrations ( $>2000 \mu\text{mol kg}^{-1}$ ) associated to relatively low temperatures ( $<26^\circ\text{C}$ ) and high salinity ( $>35$ ), are observed mainly in the SEC.

The lowest DIC values ( $<2000 \mu\text{mol kg}^{-1}$ ) are associated with high temperature and low salinity in the GC.

In the eastern equatorial Atlantic, surface water DIC increases as salinity increases and temperature decreases because of the upwelling supplying cold waters rich in  $\text{CO}_2$ .

During EGEE 5 along 2°E, the DIC ranges from 1920  $\mu\text{mol kg}^{-1}$  to 1980  $\mu\text{mol kg}^{-1}$  between the equator and 6°N with a mean value of  $1967 \pm 48 \mu\text{mol kg}^{-1}$ , and from 1983  $\mu\text{mol kg}^{-1}$  to 2050  $\mu\text{mol kg}^{-1}$  between the equator and 6°S with a mean value of  $2037 \pm 29 \mu\text{mol kg}^{-1}$ . After normalizing DIC to a salinity of 35 ( $\text{NDIC} = \text{DIC} * 35 / \text{SSS}$ ), the north-south gradient is still there (Fig. 4a), suggesting that the north-south DIC gradient cannot be solely explained by dilution processes. In addition to a

dilution effect, the impact of the cold tongue is observed with surface waters enriched in DIC south of the equator. The relatively high surface DIC can be explained by upwelling supply of  $\text{CO}_2$ -rich waters. In this region high biological activity occurs in subsurface with a maximum of fluorescence typically observed around 60 m at the EGEE CTD stations. Few high surface fluorescence values are measured near the equator at 10°W, in upwelled waters. The highest value ( $0.87 \mu\text{g L}^{-1}$ ) is observed during EGEE 1 in June 2005 at 1°N, 10°W. Averaging all the surface fluorescence data of the six cruises gives a value of  $0.12 \pm 0.15 \mu\text{g L}^{-1}$  with a mean maximum value of  $0.21 \pm 0.22 \mu\text{g L}^{-1}$  observed during EGEE 1 in June 2005 and a minimum of  $0.05 \pm 0.04 \mu\text{g L}^{-1}$  measured during EGEE 4 in November 2006. The June cruises tend to have slightly higher surface values than the September cruises. The fluorescence profile shows a maximum in subsurface, which is consistent with the Typical Tropical Structure described by [Herbland and Voituriez \(1979\)](#). Nutrients are mostly consumed at the depth of the subsurface chlorophyll maximum and very low surface values are measured ( $<1 \mu\text{mol kg}^{-1}$  for nitrates and phosphates).

In June and September, averaged DIC concentrations are respectively  $2001 \pm 53 \mu\text{mol kg}^{-1}$  and  $2006 \pm 53 \mu\text{mol kg}^{-1}$ . No significant year to year variation has been observed. North of the equator, averaged DIC value ranges from  $1962 \pm 48 \mu\text{mol kg}^{-1}$  in September to  $1973 \pm 48 \mu\text{mol kg}^{-1}$  in June. South of the equator, averaged DIC value varies from  $2034 \pm 29 \mu\text{mol kg}^{-1}$  in September to  $2042 \pm 27 \mu\text{mol kg}^{-1}$  in June (Fig. 4b and c).

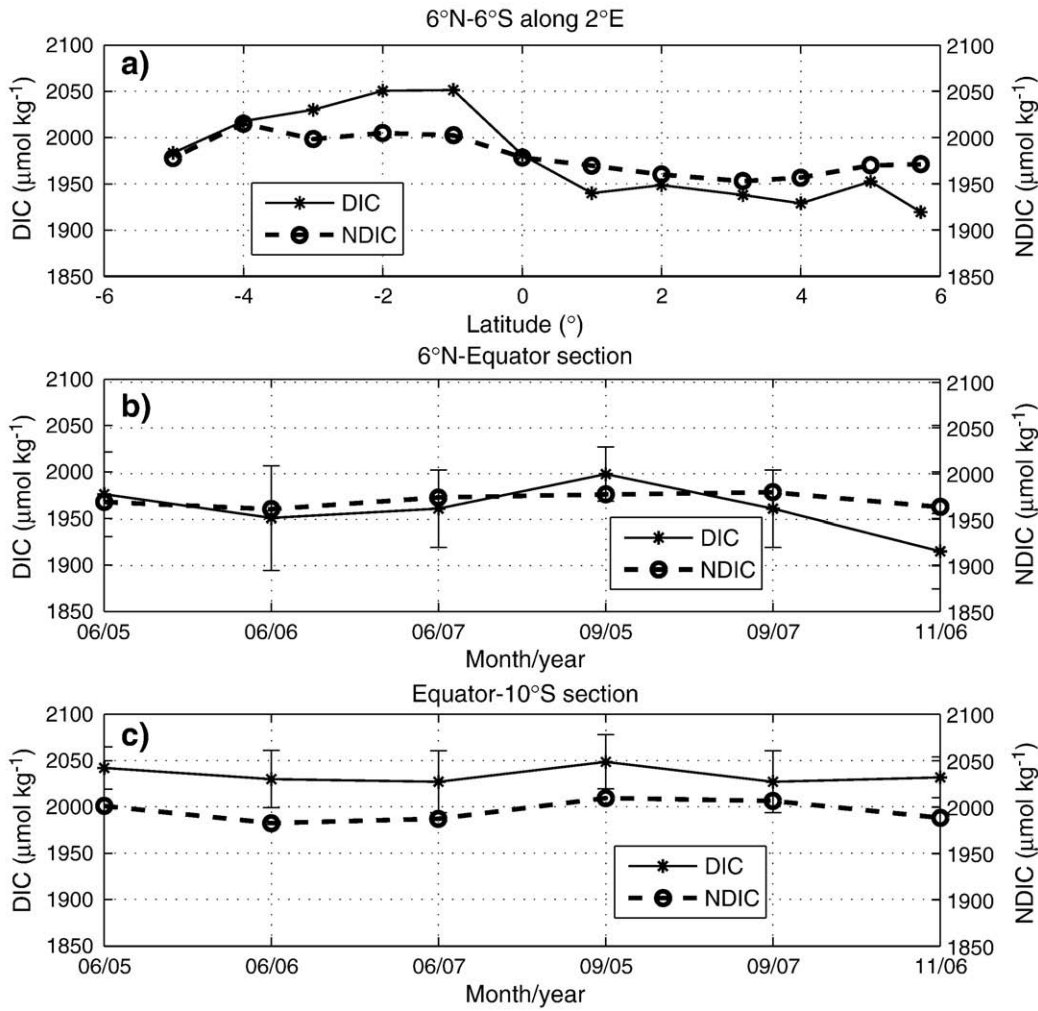


Fig. 4. a) Distribution of dissolved inorganic carbon (DIC) and normalized DIC (NDIC) between 6°N and 6°S during EGEE 5 in June 2007 along 2°E. b) Time variability of DIC and NDIC from 6°N to the equator, and c) from the equator to 10°S. Standard deviation ( $\pm 1\sigma$ ) is indicated by vertical bars.

## 5. Relationships between carbon and hydrological parameters

### 5.1. Relationship alkalinity–salinity

The whole EGEE dataset is used to determine a relationship between TA and SSS. A good correlation is obtained (Fig. 5) and the equation of the fit is given by:

$$TA = 65.52(\pm 0.77) * SSS + 2.50(\pm 27.22) \quad r^2 = 0.97. \quad (1)$$

The standard error on the predicted alkalinity is  $\pm 7.2 \mu\text{mol kg}^{-1}$ . This relationship is valid for salinity ranging from 32 to 37. Very low salinities ( $<33$ ), due to river discharge, are found at 3°N–5°N, 2°E–6°E in November 2006 and September 2007 near the coast.

In the Tropical Atlantic, several TA–SSS relationships have been proposed to derive alkalinity from SSS fields. Millero et al. (1998), Friis et al. (2003), Ríos et al. (2003) and Lefèvre et al. (2008) have proposed relationships of the form  $TA = a SSS + b$  for larger zones than the zone of EGEE cruises in the Atlantic Ocean.

These relationships have been determined for different areas (Table 2), which could explain the variability of the slope that ranges from  $50 \mu\text{mol kg}^{-1}$  to  $70 \mu\text{mol kg}^{-1}$ . In general, these relationships are valid for the salinity range of 33–37. A relationship between alkalinity, SST and salinity has been proposed for the tropical Atlantic Ocean between 30°N–30°S by Lee et al. (2006) for temperatures warmer than 20 °C and salinities between 31 and 38.

To compare these different relationships, the root mean square error (rmse) and the mean bias error (mbe) have been calculated as follows:

$$rmse = \left[ \frac{\sum (TA_{\text{obs}} - TA_{\text{fit}})^2}{(N-1)} \right]^{1/2} \quad (2)$$

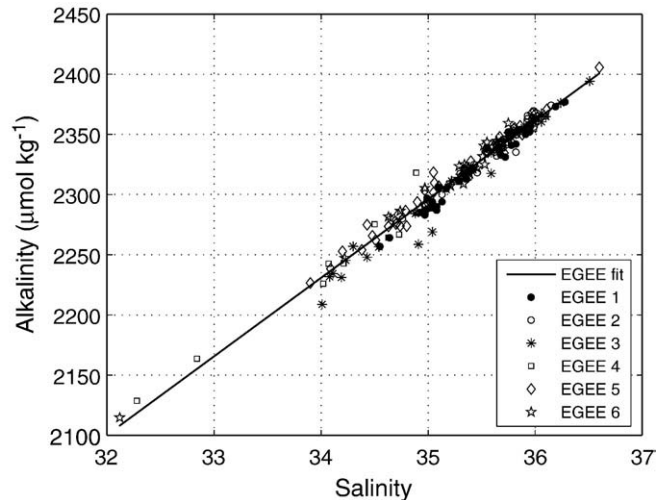


Fig. 5. TA as a function of S during the EGEE cruises. The fit is indicated by a solid line.

**Table 2**

TA–S relationships established in the Atlantic Ocean. rmse is root mean square error and mbe is mean bias error. N is the number of samples.

Area	Relationship TA–SSS–SST	N	rmse ( $\mu\text{mol kg}^{-1}$ )	mbe ( $\mu\text{mol kg}^{-1}$ )	Reference
6°N–12°S; 10°W–12°E (Atlantic Ocean)	65.52*SSS + 2.50	195	7.21	0.01	EGEE 1–6 (2005–2007)
20°N–20°S; 40°W–15°W (Atlantic Ocean)	70.73*SSS – 183.82	195	8.14	1.37	Lefèvre et al. (2008)
30°S–30°N (Atlantic, Indian, Pacific Oceans)	2305 + 58.66*(SSS – 35) + 2.32*(SSS – 35) <sup>2</sup> – 1.41*(SST – 20) + 0.04*(SST – 20) <sup>2</sup>	195	8.42	–1.55	Lee et al. (2006)
31°N–12.5°S (Atlantic Ocean)	58.47*SSS + 253	195	8.75	–1.40	Friis et al. (2003)
10°N–33°S; 20°W–15°E (Atlantic Ocean)	70.35*SSS – 166	195	8.17	–2.02	Ríos et al. (2003)
80°N–60°S (Atlantic Ocean)	51.24*SSS + 520.1	195	17.83	–13.12	Millero et al. (1998)

$$mbe = [\sum(TA_{obs} - TA_{fit}) / N] \quad (3)$$

where  $TA_{obs}$  is the observed value,  $TA_{fit}$  is the predicted value by the TA–S equation and  $N$  is the number of samples.

Each relationship has been compared with the EGEE TA measurements (Table 2). The rmse ranges between 7 and 18  $\mu\text{mol kg}^{-1}$ . Among the five relationships, the one determined by Millero et al. (1998) gives the highest rmse (almost twice the averaged rmse) and an mbe of about 13  $\mu\text{mol kg}^{-1}$ . The relationships with a slope between 65 and 70  $\mu\text{mol kg}^{-1}$  provide the smallest rmse.

The ARAMIS cruises crossed the equator around 25°W in October 2005, May 2006 and April 2007 and these data were not used to determine the TA–SSS relationship so they can be used to check whether Eq. (1) is valid further west. Using the ARAMIS data, the smallest rmse (10.87  $\mu\text{mol kg}^{-1}$ ) is obtained with the EGEE relationship suggesting that Eq. (1) can be applied in the tropical Atlantic on a larger area than the eastern equatorial Atlantic.

### 5.2. Relationship DIC–temperature–salinity

The variability of the carbon parameters in the eastern equatorial Atlantic depends strongly on the current system. The lowest DIC is observed in the GC region whereas the SEC region exhibits higher DIC. As a water mass is characterized by its temperature and salinity, we used SST and SSS observations from EGEE 1 to 6 to determine a relationship between DIC and both SSS and SST. At first, two zones were considered according to the observed north–south gradient.

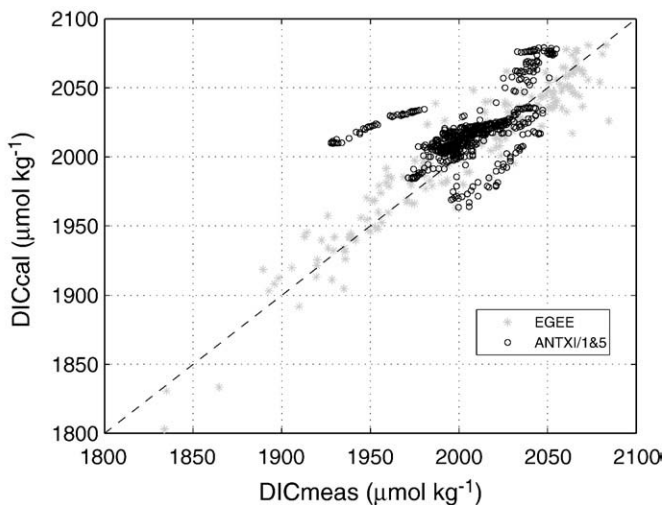


**Fig. 6.** Comparison between calculated and measured DIC using data from EGEE (asterisk), ANT XI/1&5 (open circle),  $y=x$  (dashed line).

However, the two relationships obtained did not significantly improve the estimate of DIC so the whole dataset was used.

The following equation has been obtained in the salinity range of 32–37:

$$DIC = (51.71 \pm 2.16) * SSS + (-12.79 \pm 0.89) * SST + (507.82 \pm 91.32) \quad r^2 = 0.90. \quad (4)$$

The standard error on the predicted DIC is  $\pm 16.6 \mu\text{mol kg}^{-1}$ . The variability of DIC is explained at 90% by the effects of temperature and salinity. Adding the fluorescence would slightly improve the fit ( $r^2 = 0.94$ ). However, as fluorescence and SST are correlated ( $r^2 = 0.42$ ), we can assume that the biology is taken into account by the SST. Low SST is associated with relatively high surface fluorescence.

Lefèvre et al. (2008) determined a DIC–SST relationship for June–September 2006 using data recorded at the 6°S, 10°W mooring. If we use this relationship to remove the upwelling effect, the remaining DIC is strongly correlated to salinity with 76% of the DIC variability explained by salinity.

The scatter plot of the measured DIC versus calculated DIC is shown on Fig. 6. The low calculated DIC ( $< 1850 \mu\text{mol kg}^{-1}$ ) correspond to very low salinities ( $< 33$ ). To examine the robustness of this relationship with independent measurements, the DIC estimates are compared with measurements performed during ANT XI/1&5 from 10°W to 10°E and from 10°S to 6°N (Fig. 6). Overall, the rmse (26.03  $\mu\text{mol kg}^{-1}$ ) and the mbe ( $-12.75 \mu\text{mol kg}^{-1}$ ) obtained during ANT XI/1&5 are, in absolute value, higher than the ones obtained using the EGEE data. However, a set of DIC measurements (from 1930  $\mu\text{mol kg}^{-1}$  to 1980  $\mu\text{mol kg}^{-1}$ ) is far from the regression line. They are located between 10°W and 8°W at 2°S in October–November 1993. In this area, averaged SST, averaged SSS and averaged DIC during ANT XI/1&5 are respectively  $26.32 \pm 0.39$  °C,  $35.85 \pm 0.09$  and  $1957 \pm 17 \mu\text{mol kg}^{-1}$ . Very similar SSS and SST are observed during the same cruise at 2°E, 4°S for which observed DIC are in good agreement with calculated DIC (difference less than 10  $\mu\text{mol kg}^{-1}$ ). Therefore, the large difference at 2°S is likely due to a local dynamical or biological feature not taken into account in our regression. If we remove this local feature, the mbe becomes  $-8 \mu\text{mol kg}^{-1}$  and the rmse 16.6  $\mu\text{mol kg}^{-1}$ , a value comparable to the rmse obtained with the

**Table 3**

Comparison of different constants of dissociation used to calculate the fugacity of  $\text{CO}_2$ .

Constants of dissociation	rmse $f\text{CO}_2$ (mes-calc) ( $\mu\text{atm}$ )	Mean $f\text{CO}_2$ (mes-calc) ( $\mu\text{atm}$ )
Peng	14.76	–12.78
Roy	31.64	–29.86
Mehr, refit D&M87	7.32	3.76
Mehr–Hans, refit D&M	20.50	–7.88
Hans, refit D&M	17.90	–16.00
Goyet and Poisson	28.13	–26.38

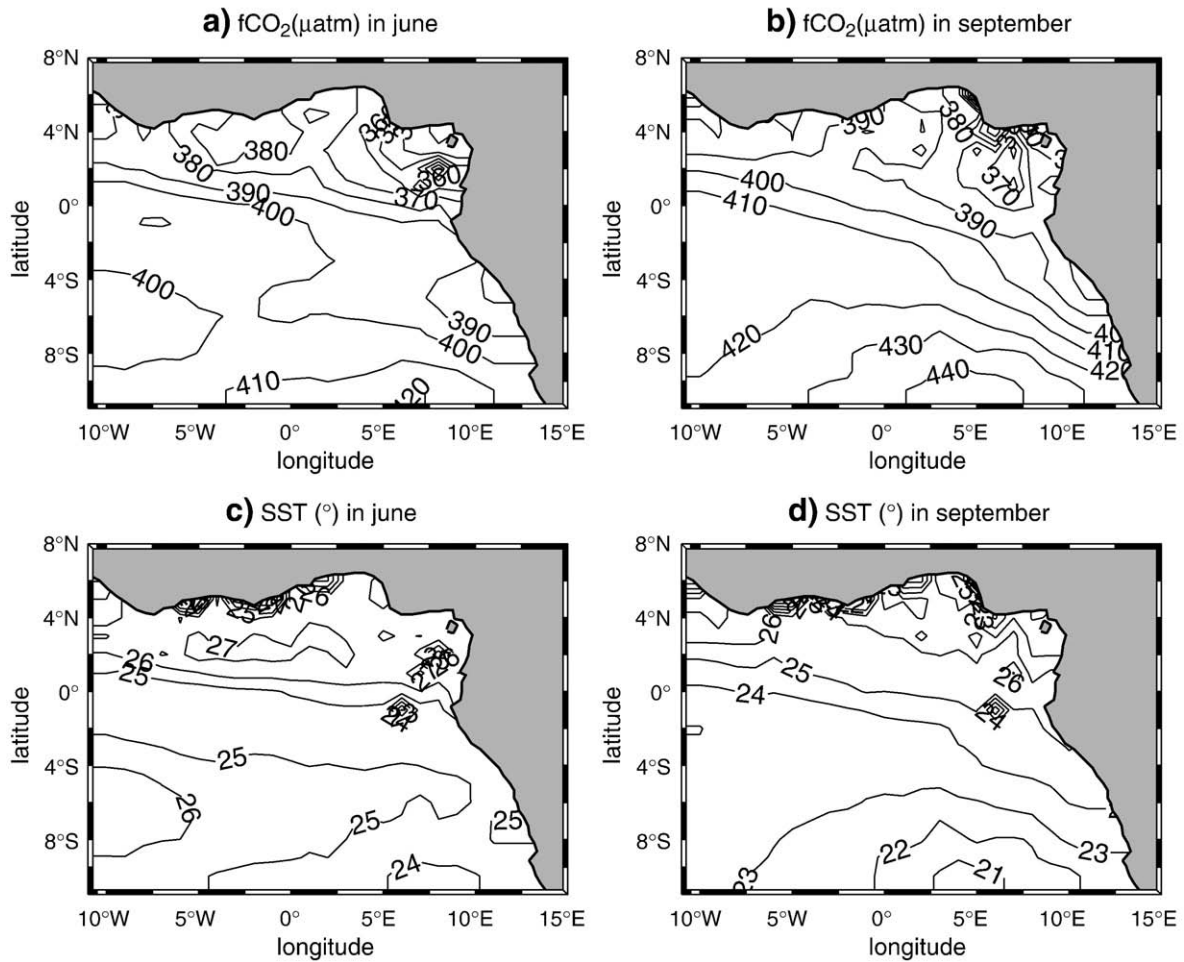


Fig. 7. a) Distribution of the fugacity of CO<sub>2</sub> (fCO<sub>2</sub>) in June, b) in September, and distribution of SST c) in June and d) in September.

EGEE data. Taking into account the 12 years lag between the ANTIXI/1&5 and the EGEE cruises, the obtained mbe corresponds to an increase of DIC of  $0.7 \mu\text{mol kg}^{-1} \text{year}^{-1}$ . This is comparable to a DIC increase following the atmospheric fCO<sub>2</sub> increase: considering a Revelle factor of 9 and an atmospheric fCO<sub>2</sub> increase of  $1.6 \mu\text{atm year}^{-1}$  (as recorded by the atmospheric station located at Ascension Island,  $7.92^\circ\text{S}$ ,  $14.42^\circ\text{W}$ ), the rate of DIC increase is expected to be  $0.9 \mu\text{mol kg}^{-1} \text{year}^{-1}$ . Therefore, taken into account the time lag between the ANTIXI and EGEE cruises, the DIC measured during the ANTIXI/1 & 5 cruises are relatively well reproduced by Eq. (4).

## 6. fCO<sub>2</sub> and air-sea CO<sub>2</sub> flux in the eastern equatorial Atlantic

### 6.1. Calculation of fCO<sub>2</sub> from DIC and TA leading to monthly maps

The oceanic fCO<sub>2</sub> calculated from measured DIC and TA, using different constants of dissociation, has been compared to underway fCO<sub>2</sub> measured during the EGEE 3 cruise. The dissociation constants of Mehrbach et al. (1973) refitted by Dickson and Millero (1987) give the best results (Table 3). In the following, we use these constants.

TA and DIC have been calculated in the eastern equatorial Atlantic with Eqs. (1) and (4) using monthly mean SSS fields from the *World Ocean Atlas 2005* on a  $1^\circ$  latitude  $\times$   $1^\circ$  longitude grid (Antonov et al., 2006) and using SST from the TRMM (*Tropical Rain Mission Measurements*) *Microwave Imager* on a  $0.25^\circ$  latitude  $\times$   $0.25^\circ$  longitude grid from 2005 to 2007. The monthly fCO<sub>2</sub> and SST maps are presented for June and September on a

$1^\circ \times 1^\circ$  grid (Fig. 7). Overall, the lowest fCO<sub>2</sub> (340–390  $\mu\text{atm}$ ) is located between  $6^\circ\text{N}$ – $0^\circ\text{N}$  and  $10^\circ\text{W}$ – $10^\circ\text{E}$  in the GC and the highest fCO<sub>2</sub> is located in the SEC. The averaged fCO<sub>2</sub>, in the eastern equatorial Atlantic, ranges from  $393 \pm 16 \mu\text{atm}$  in June to  $408 \pm 18 \mu\text{atm}$  in September. This slight fCO<sub>2</sub> increase is associated with the decrease of SST from  $25.47 \pm 0.93^\circ\text{C}$  in June to  $23.87 \pm 1.28^\circ\text{C}$  in September (Fig. 7c and d).

From  $6^\circ\text{N}$  to the equator, averaged fCO<sub>2</sub> ranges from  $375 \pm 17 \mu\text{atm}$  in June to  $389 \pm 12 \mu\text{atm}$  in September. For comparison, averaging the underway fCO<sub>2</sub> measured during EGEE 3 in June 2006 gives  $381 \pm 20 \mu\text{atm}$  and the climatology of Takahashi et al. (2009) gives  $382 \mu\text{atm}$ . Given the variability of fCO<sub>2</sub> in this region, the mean values are in good agreement.

From the equator to  $10^\circ\text{S}$ , averaged fCO<sub>2</sub> is higher and varies from  $400 \pm 8 \mu\text{atm}$  in June to  $415 \pm 15 \mu\text{atm}$  in September. fCO<sub>2</sub> increases from the north of the equator to  $10^\circ\text{S}$  during these two months. fCO<sub>2</sub> follows the trend of SSS but varies in an opposite way to temperature. The mean value of underway fCO<sub>2</sub> measured during EGEE 3 is  $411 \pm 29 \mu\text{atm}$  in June 2006 whereas the climatology gives a lower value of  $386 \mu\text{atm}$ . High fCO<sub>2</sub> south of the equator results from the upwelling, and the warming of the surface waters within the SEC might increase fCO<sub>2</sub> even further.

### 6.2. Comparison with other estimates

Underway fCO<sub>2</sub> measured during EGEE 3 in June 2006 is compared with calculated fCO<sub>2</sub> from TA and DIC using Eqs. (1) and (4), and

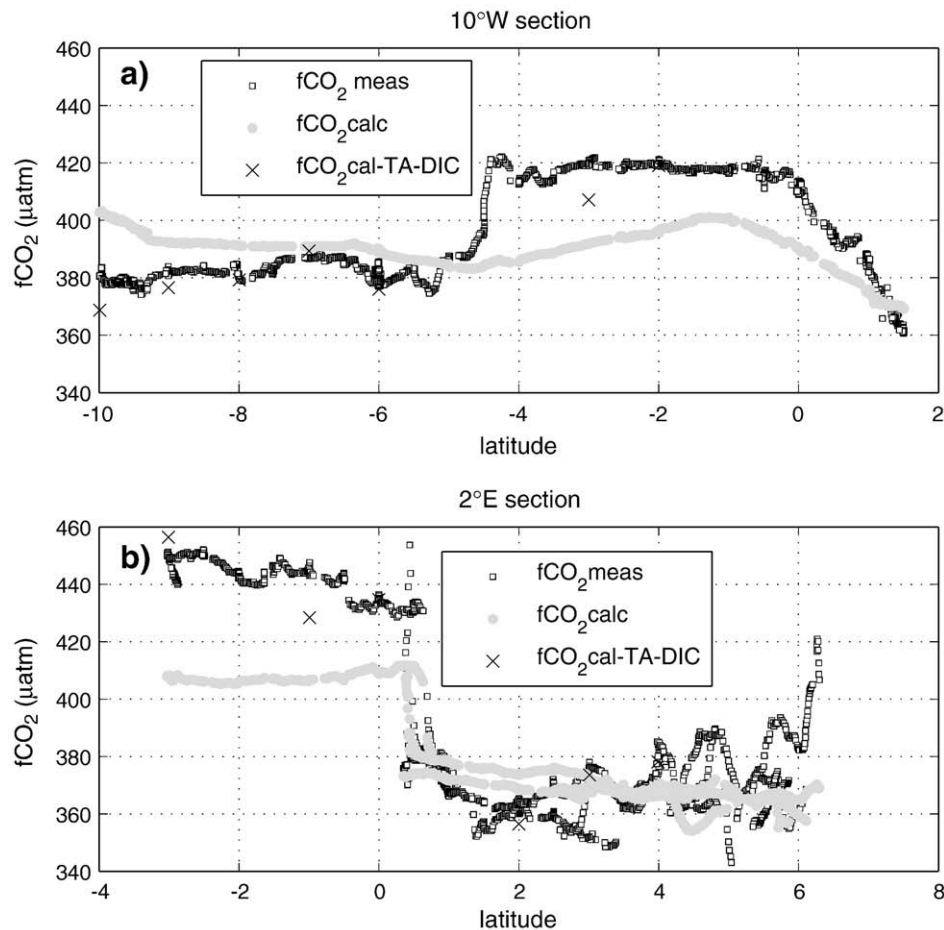


Fig. 8. Comparison between measured and calculated  $f\text{CO}_2$  during the EGEE 3 cruise: a) along  $10^\circ\text{W}$  and b) along  $2^\circ\text{E}$ .

calculated  $f\text{CO}_2$  from measured DIC and TA along the  $10^\circ\text{W}$  and  $2^\circ\text{E}$  sections (Fig. 8).  $f\text{CO}_2$  values calculated from measured DIC and TA agree well with measured  $f\text{CO}_2$ . Discrepancies arise when using Eqs. (1) and (4) to calculate DIC and TA and then  $f\text{CO}_2$ . Measured and calculated  $f\text{CO}_2$  are in good agreement between  $6^\circ\text{N}$  and  $0.5^\circ\text{N}$  along the  $2^\circ\text{E}$  section ( $\text{rmse} = 11.3 \mu\text{atm}$  and  $\text{mbe} = 0.4 \mu\text{atm}$ ) and between  $4.5^\circ\text{S}$  and  $10^\circ\text{S}$  along the  $10^\circ\text{W}$  section ( $\text{rmse} = 11.60 \mu\text{atm}$  and  $\text{mbe} = -9.80 \mu\text{atm}$ ), (Fig. 8). On the other hand, large biases are observed along  $2^\circ\text{E}$  south of  $0.5^\circ\text{N}$  ( $\text{rmse} = 34.2 \mu\text{atm}$  and  $\text{mbe} = 31.8 \mu\text{atm}$ ) and along  $10^\circ\text{W}$  between  $4.5^\circ\text{S}$  and  $2^\circ\text{N}$  ( $\text{rmse} = 20.3 \mu\text{atm}$  and  $\text{mbe} = 17.6 \mu\text{atm}$ ) with calculated  $f\text{CO}_2$  lower than measured values. The difference between measured and calculated  $f\text{CO}_2$  ranges from  $20 \mu\text{atm}$  to  $40 \mu\text{atm}$  between  $0.5^\circ\text{N}$  and  $4.5^\circ\text{S}$  in the SEC. In this area, the DIC relationship is not well constrained by the EGEE data, which might explain the discrepancy. In addition, the propagation of the errors made on estimated DIC and TA from the relationships contributes to the  $f\text{CO}_2$  differences between calculated and measured values.

The  $f\text{CO}_2$  distribution derived from the relationships is then compared to the climatology of Takahashi et al. (2009) along the  $10^\circ\text{W}$  and  $2^\circ\text{E}$  sections between  $2^\circ\text{N}$  and  $10^\circ\text{S}$  (Fig. 9). The climatological  $f\text{CO}_2$  values, originally referenced to the year 2000, have been corrected to the year 2006 using a mean rate of surface seawater  $f\text{CO}_2$  increase of  $1.5 \mu\text{atm year}^{-1}$ . Thus,  $9 \mu\text{atm}$  has been added to the climatological  $f\text{CO}_2$ . The climatology gives lower values than the calculated  $f\text{CO}_2$  (Fig. 9) which already underestimated the measured values in June along  $2^\circ\text{E}$  and  $10^\circ\text{W}$ . The best agreement between climatological  $f\text{CO}_2$  and the calculated  $f\text{CO}_2$  is observed in June with a difference ranging from  $-20 \mu\text{atm}$  to  $+20 \mu\text{atm}$ . On

average the difference climatology-estimated  $f\text{CO}_2$  in June is  $-11 \mu\text{atm}$ . The largest disagreement is observed in September along  $2^\circ\text{E}$  in the south with differences reaching  $-60 \mu\text{atm}$  (Fig. 9d).

Averaged SSS and SST are respectively  $35.80 \pm 0.29$  and  $21.90 \pm 0.52 \text{ }^\circ\text{C}$  from  $6^\circ\text{S}$  to  $10^\circ\text{S}$  along  $2^\circ\text{E}$  compared to the climatological SSS and SST of  $35.87$  and  $22.14 \text{ }^\circ\text{C}$ . The difference between  $f\text{CO}_2$  derived from the EGEE relationships and the climatology cannot be attributed to a difference in hydrological parameters. It is noticeable that our estimated  $f\text{CO}_2$  are almost always higher than the climatology.

Between  $1.5^\circ\text{N}$  and  $2^\circ\text{S}$ , in June, our estimated  $f\text{CO}_2$  increases from  $390 \mu\text{atm}$  to  $410 \mu\text{atm}$  corresponding to higher  $f\text{CO}_2$  in the cold tongue during the upwelling period (Fig. 9a). The climatological  $f\text{CO}_2$  is  $388 \mu\text{atm}$  and remains almost constant. In the climatology, the effect of the cold tongue is not detected probably because of the lack of data. In addition, the spatial resolution of  $4^\circ$  (latitude)  $\times$   $5^\circ$  (longitude) used in the climatology will tend to smooth the differences between northern and southern waters. On Fig. 8b the north-south transition is around  $0.5^\circ\text{N}$  and the corresponding pixel of the climatology extends from  $2^\circ\text{S}$  to  $2^\circ\text{N}$  so the resulting  $f\text{CO}_2$  is a mixture of  $\text{CO}_2$  rich and  $\text{CO}_2$  poor waters.

### 6.3. Air-sea $\text{CO}_2$ fluxes

The  $\text{CO}_2$  flux, averaged from June to November, is  $0.78 \pm 0.87 \text{ mmol m}^{-2} \text{ day}^{-1}$  between  $6^\circ\text{N}$  and the equator, and  $2.90 \pm 1.33 \text{ mmol m}^{-2} \text{ day}^{-1}$  between the equator and  $10^\circ\text{S}$ . The north-south gradient observed in  $f\text{CO}_2$  still remains as the patterns of the flux are mainly driven by oceanic  $f\text{CO}_2$ .

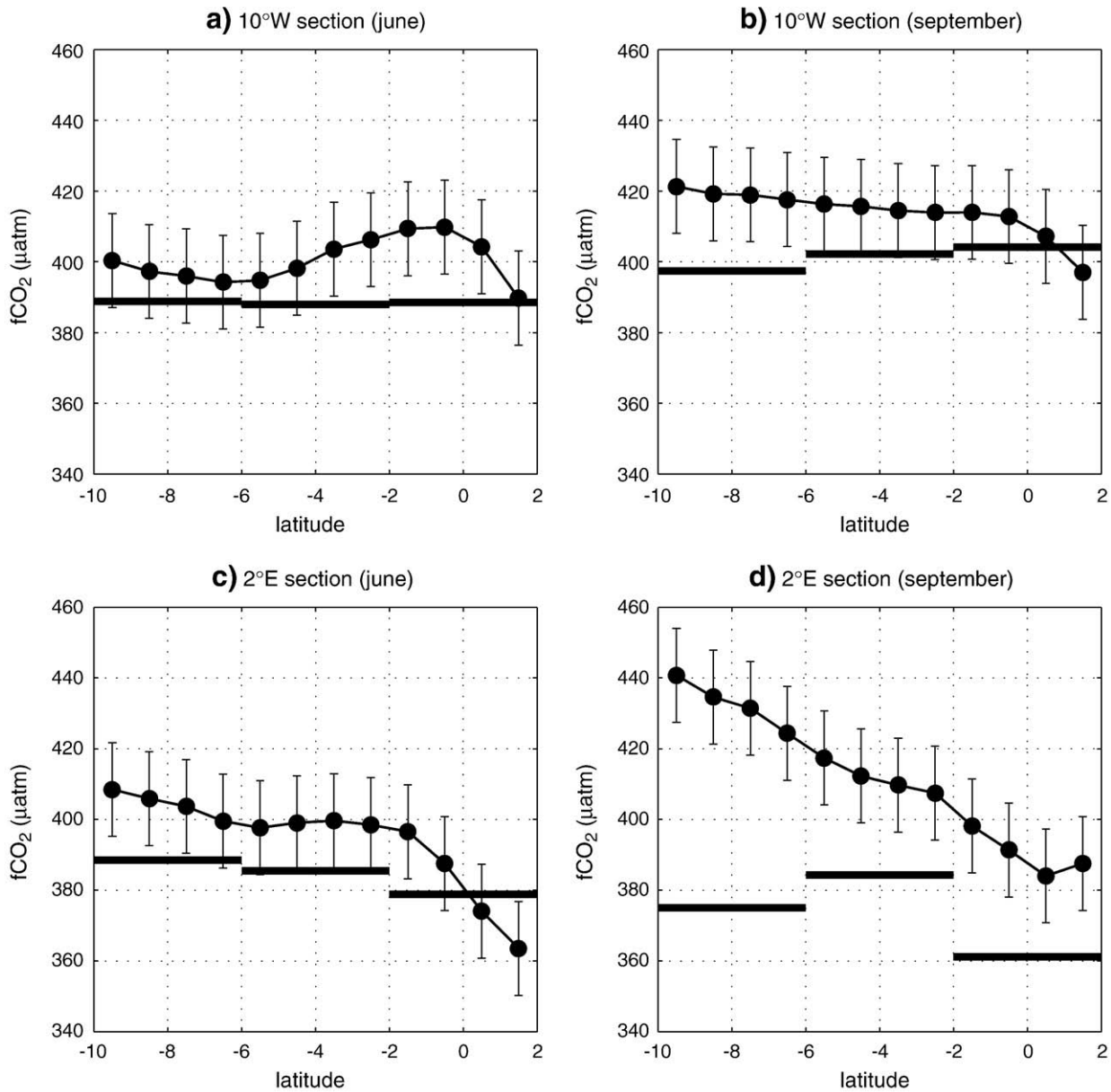


**Fig. 9.** Estimated fCO<sub>2</sub> (circles) and climatological fCO<sub>2</sub> (solid line) between 10°S and 2°N along 10°W a) in June and b) in September and along 2°E c) in June and d) in September. Standard deviation ( $\pm 1\sigma$ ) is indicated by vertical bars.

North of the equator, the CO<sub>2</sub> flux ranges from  $-0.26 \pm 1.04 \text{ mmol m}^{-2} \text{ day}^{-1}$  to  $1.35 \pm 1.53 \text{ mmol m}^{-2} \text{ day}^{-1}$  between June and November. Between the equator and 10°S, the monthly CO<sub>2</sub> flux ranges from  $2.48 \pm 1.02 \text{ mmol m}^{-2} \text{ day}^{-1}$  to  $3.35 \pm 1.46 \text{ mmol m}^{-2} \text{ day}^{-1}$ .

Using the  $\Delta f\text{CO}_2$  of the climatology of Takahashi et al. (2009) and the gas exchange coefficient used for our flux calculations, we recalculate a climatological CO<sub>2</sub> flux so that differences between the flux estimates can be attributed neither to the formulation of the gas exchange coefficient nor to the wind speed. The climatological mean flux from June to November is  $0.95 \pm 0.50 \text{ mmol m}^{-2} \text{ day}^{-1}$ , which is lower than our estimate of  $2.30 \pm 1.55 \text{ mmol m}^{-2} \text{ day}^{-1}$ . This is explained by the  $\Delta f\text{CO}_2$  values higher than the values of the climatology.

Averaged from June to November, the climatological mean flux ranges from  $0.70 \pm 0.57 \text{ mmol m}^{-2} \text{ day}^{-1}$  north of the equator to  $1.08 \pm 0.42 \text{ mmol m}^{-2} \text{ day}^{-1}$  south of the equator. The flux is very close to

our estimate of  $0.78 \pm 0.87 \text{ mmol m}^{-2} \text{ day}^{-1}$  north of the equator. South of the equator, the climatological mean flux is two times smaller than our result which is expected as the north–south gradient is not well reproduced by the climatology. Both estimates show that the eastern equatorial Atlantic always acts as a source of CO<sub>2</sub>.

## 7. Conclusions

From 2005 to 2007, TA and DIC have been measured during the EGEE cruises from June to November in the eastern equatorial Atlantic. The surface distributions of TA, DIC, SST and SSS present a north–south gradient with low alkalinity and low dissolved inorganic carbon associated with low SSS and high SST, found in the GC located north of the equator. High DIC and TA are observed south of the equator in the SEC. After normalizing DIC and TA to a salinity of 35, a slight gradient is still observed on DIC with higher values south of the equator. This suggests that the variability of alkalinity is fully

explained by the salinity variations whereas, south of the equator, DIC is supplied by upwelling waters.

Relationships between TA and SSS, and between DIC and both SST and SSS have been determined using the whole dataset. The calculated  $f\text{CO}_2$  is in reasonable agreement with the underway measurements of  $f\text{CO}_2$  made during the EGEE 3 cruise in June 2006 along 2°E between 6°N and 0.5°N and along 10°W between 4.5°S and 10°S. Between 4.5°S and 0.5°S, our calculated  $f\text{CO}_2$  is always lower than the measurements, which may lead to an underestimate of the  $\text{CO}_2$  outgassing in this area.

Using SSS and SST fields, monthly maps of  $f\text{CO}_2$  have been constructed from 2005 to 2007 for the June to November months. The  $\text{CO}_2$  flux has then been calculated over that period. The eastern equatorial Atlantic is a source of  $\text{CO}_2$  throughout the year and the north–south gradient is still observed as the flux pattern depends mainly on  $\Delta f\text{CO}_2$ . The monthly mean  $\text{CO}_2$  flux, south of the equator, is four times higher than the flux in the north, whereas there is no significant north–south difference according to the Takahashi et al.'s (2009) climatology. The north–south gradient is missed by the climatology possibly due to a combination of lack of data and coarse resolution.

The TA and DIC relationships could be improved by increasing the measurements between 4°S and 10°S. In addition, this study is limited to the June–November period because of the lack of measurements for the rest of the year. It is therefore critical to take measurements from December to May in order to study the seasonal cycle in this region.

## Acknowledgements

We thank Nicolas Metzl for helpful comments. The EGEE/AMMA project is coordinated by Bernard Bourlès, of Institut de Recherche pour le Développement (IRD) Brest. We thank the crew members of the N/O Antea for their help during the cruise. TMI data are produced by Remote Sensing Systems and sponsored by the NASA Earth Science and REASON DISCOVER project. They are available at [www.remss.com](http://www.remss.com). DIC and TA analyses have been performed by the service national d'analyses des paramètres du  $\text{CO}_2$  (SNAPO- $\text{CO}_2$ ) at the LOCEAN laboratory. U. Koffi is supported by a Ph-D fellowship from the Département Soutien et Formation (DSF) at IRD. This work is funded by the European Integrated Project CARBOOCEAN (contract 51176-2). This manuscript benefited from the comments of three anonymous reviewers.

## References

Andrié, C., Oudot, C., Genthon, C., 1986.  $\text{CO}_2$  fluxes in the tropical Atlantic during focal cruises. *J. Geophys. Res.* 91, 11741–11755.

Antonov, J.I., Locarnini, R.A., Boyer, T.P., Mishonov, A.V., Garcia, H.E., 2006. World Ocean Atlas 2005, volume 2: salinity. In: Levitus, S. (Ed.), NOAA Atlas NESDIS, 62. U. S. Government Printing Office, D. C., 182 pp.

Baker, D.F., Law, R.M., Gurney, K.R., Rayner, P., Peylin, P., Denning, A.S., Bousquet, P., Bruhwiler, L., Chen, Y.-H., Ciais, P., Fung, I.Y., Heimann, M., John, J., Maki, T., Maksyutov, S., Masarie, K., Prather, M., Pak, B., Taguchi, S., Zhu, Z., 2006. TransCom 3 inversion intercomparison: impact of transport model errors on the interannual variability of regional  $\text{CO}_2$  fluxes, 1988–2003. *Glob. Biogeochem. Cycles* 20, GB1002. doi10.1029/2004GB002439.

Bakker, D.C.E., de Baar, H.J.W., de Jong, E., 1999. The dependence on temperature and salinity of dissolved inorganic carbon in East Atlantic surface waters. *Mar. Chem.* 65, 263–280.

Binet, D., Marchal, E., 1993. The Large Marine Ecosystem of the Gulf of Guinea: longterm variability induced by climatic changes. In: Sherman, K., Alexander, L.M., Gold, B. (Eds.), *Large Marine Ecosystems – Stress, Mitigation and Sustainability*. American Association for the Advancement of Science, Washington D.C., pp. 104–118.

Boutin, J., Quilfen, Y., Merlivat, L., Piollet, J.F., 2009. Global average of air–sea  $\text{CO}_2$  transfer velocity from QuikSCAT scatterometer wind speeds. *J. Geophys. Res.* 114, C04007. doi10.1029/2007JG004168.

D.O.E. (U.S. Department of Energy), 1994. Handbook of methods for analysis of the various parameters of the carbon dioxide system in sea water; version 2. In: Dickson, A.G., Goyet, C. (Eds.), ORNL/CDIAC - 74. A.G.

Denman, K.L., Brasseur, G., Chidthaisong, A., Ciais, P., Cox, P.M., Dickinson, R.E., Hauglustaine, D., Heinze, C., Holland, E., Jacob, D., Lohmann, U., Ramachandran, S., da Silva Dias, P.L., Wofsy, S.C., Zhang, X., 2007. Couplings between changes in the climate system and biogeochemistry. In: Solomon, S., Qin, D., Manning, M., Chen, Z., Marquis, M., Averyt, K.B., Tignor, M., Miller, H.L. (Eds.), *Climate Change 2007: The Physical Basis. Contribution of Working Group I to the Fourth Assessment Report of the Intergovernmental Panel on Climate Change*. Cambridge university press, Cambridge.

Dickson, A.G., Millero, F.J., 1987. A comparison of the equilibrium constants for the dissociation of carbonic acid in seawater media. *Deep-Sea Res.* 34 (10), 1733–1743.

Edmond, J.M., 1970. High precision determination of titration alkalinity and total carbon dioxide content of seawater by potentiometric titration. *Deep-Sea Res.* 17 (4), 737–750.

Friis, K., Körtzinger, A., Wallace, D.W.R., 2003. The salinity normalization of marine inorganic carbon chemistry data. *Geophys. Res. Lett.* 30 (2), 1085. doi10.1029/2002GL015898.

Gruber, N., Gloor, M., Fletcher, S.E.M., Doney, S.C., Dutkiewicz, S., Follows, M.J., Gerber, M., Jacobson, A.R., Joos, F., Lindsay, K., Menemenlis, D., Mouchet, A., Müller, S.A., Sarmiento, J.L., Takahashi, T., 2009. Oceanic sources, sinks, and transport of atmospheric  $\text{CO}_2$ . *Glob. Biogeochem. Cycles* 23 (1), GB1005. doi10.1029/2008GB003349.

Hardman-Mountford, N.J., McGlade, J.M., 2003. Seasonal and interannual variability of oceanographic processes in the Eastern equatorial Atlantic: an investigation using AVHRR sea surface temperature data. *Int. J. Remote Sens.* 24 (16), 3247–3268.

Herbland, A., Voituriez, B., 1979. Hydrological structure analysis for estimating the primary production in the tropical Atlantic Ocean. *J. Mar. Res.* 37, 87–101.

Lee, K., Tong, L.T., Millero, F.J., Sabine, C.L., Dickson, A.G., Goyet, C., Park, G.H., Wanninkhof, R., Feely, R.A., Key, R.M., 2006. Global relationships of total alkalinity with salinity and temperature in surface waters of the world's oceans. *Geophys. Res. Lett.* 33, L19605. doi10.1029/2006GL027207.

Lefèvre, N., 2009. Low  $\text{CO}_2$  concentrations in the Gulf of Guinea during the upwelling season in 2006. *Mar. Chem.* 113, 93–101. doi10.1016/j.marchem.2009.01.001.

Lefèvre, N., Guillot, A., Beaumont, L., Danguy, T., 2008. Variability of  $f\text{CO}_2$  in the Eastern Tropical Atlantic from a moored buoy. *J. Geophys. Res.* 113, C01015. doi10.1029/2007JC004146.

Mehrbach, C., Culbertson, C.H., Hawley, J.E., Pytkowicz, R.M., 1973. Measurement of the apparent dissociation constants of carbonic acid in seawater at atmospheric pressure. *Limnol. Oceanogr.* 18, 897–907.

Millero, F., Lee, K., Roche, M., 1998. Distribution of alkalinity in the surface waters of the major oceans. *Mar. Chem.* 60, 111–130.

Oudot, C., Ternon, J.F., Lecomte, J., 1995. Measurements of atmospheric and oceanic  $\text{CO}_2$  in the tropical Atlantic: 10 years after the 1982–1984 FOCAL cruises. *Tellus* 47B, 70–85.

Ríos, A.F., Alvarez-Salgado, X.A., Pérez, F.F., Bingler, L.S., Aristegui, J., Mémerly, L., 2003. Carbon dioxide along WOCE line A14: water masses characterization and anthropogenic entry. *J. Geophys. Res.* 108 (C4), 3123. doi10.1029/2000JC000366.

Stramma, L., Schott, F., 1999. The mean flow field of the tropical Atlantic Ocean. *Deep-Sea Res.* II 46, 279–303.

Sweeney, C., Gloor, E., Jacobson, A.R., Key, R.M., McKinley, G., Sarmiento, J.L., Wanninkhof, R., 2007. Constraining global air–sea gas exchange for  $\text{CO}_2$  with recent bomb  $^{14}\text{C}$  measurements. *Glob. Biogeochem. Cycles* 21, GB2015. doi10.1029/2006GB002784.

Takahashi, T., Sutherland, C.S., Wanninkhof, R., Sweeney, C., Feely, R.A., Chipman, D.W., Hales, B., Friederich, G., Chavez, F., Sabine, C., Watson, A., Bakker, D.C.E., Schuster, U., Metzl, N., Inoue, H.Y., Ishii, M., Midorikawa, T., Nojiri, Y., Körtzinger, A., Steinhoff, T., Hoppema, M., Olafsson, J., Arnarson, T.S., Tilbrook, B., Johannessen, T., Olsen, A., Bellerby, R., Wong, C.S., Delille, B., Bates, N.R., de Baar, H.J.W., 2009. Climatological mean and decadal change in surface ocean  $\text{pCO}_2$ , and net sea–air  $\text{CO}_2$  flux over the global oceans. *Deep-Sea Res.* II 56, 554–577. doi10.1016/j.dsr2.2008.12.009.

Tanguy, Y., Arnault, S., Lattes, P., 2010. Isothermal, mixed, and barrier layers in the subtropical and tropical Atlantic Ocean during the ARAMIS experiment. *Deep-Sea Res.* I 57, 501–517.